





Multi-messenger Extended Emission from the Compact Remnant in GW170817

Maurice H. P. M. van Putten¹ , Massimo Della Valle^{2,3} , and Amir Levinson⁴¹Sejong University, 98 Gunja-Dong Gwangin-gu, Seoul 143-6%747, Republic of Korea; mvp@sejong.ac.kr²Instituto Nazionale di Astrofisica, Osservatorio Astronomico di Capodimonte, Salita Moiariello 16, I-80131 Napoli, Italy³ESO, D-85748, Garching bei München, Germany⁴School of Physics and Astronomy, Tel Aviv University, 69978 Tel Aviv, Israel

Received 2019 January 30; revised 2019 April 10; accepted 2019 April 12; published 2019 April 25

Abstract

GW170817/GRB 170817A probably marks a double neutron star (NS) coalescence. Extended emission $t_s \simeq (0.67 \pm 0.03)$ s post-merger shows an estimated energy output $\mathcal{E} \simeq (3.5 \pm 1)\%M_\odot c^2$ determined by response curves to power-law signal injections, where c is the velocity of light. It provides calorimetric evidence for a rotating black hole of $\sim 3M_\odot$, inheriting the angular momentum J of the merged hyper-massive NS in the immediate aftermath of GW170817 following core-collapse about or prior to t_s . Core-collapse greatly increases the central energy reservoir to $E_j \lesssim 1M_\odot c^2$, accounting for \mathcal{E} even at modest efficiencies in radiating gravitational waves through a non-axisymmetric thick torus. The associated multi-messenger output in ultra-relativistic outflows and sub-relativistic mass-ejecta is consistent with observational constraints from the gamma-ray burst afterglow emission of GRB 170817A and accompanying kilonova.

Key words: gamma-ray burst: individual (GRB 170817A) – gravitational waves – methods: data analysis – stars: black holes – stars: neutron

1. Introduction

The observation of GW170817 (Abbott et al. 2017a, 2017b) was the first observation of a low-mass compact binary coalescence seen in a long-duration ascending gravitational-wave (GW) chirp. The accompanying GRB 170817A, identified by the *Fermi*-Gamma-Ray Burst Monitor (GBM) and the *INTErnational Gamma-Ray Astrophysics Laboratory* (*INTEGRAL*; Connaughton 2017; Goldstein et al. 2017; Kasliwal et al. 2017; Savchenko et al. 2017; Pozanenko et al. 2018), represents the merger of either a neutron star (NS) with another neutron star (NS–NS) or with a companion black hole (BH; NS–BH) with a chirp mass of about one solar mass. The potentially broad implications of the former has received considerable attention because of what it reveals about the origin of heavy elements (D’Avanzo et al. 2017; Kasen et al. 2017; Pian et al. 2017; Smartt et al. 2017) as well as entirely novel measurements of the Hubble constant (Freedman 2017; Guidorzi et al. 2017).

Regarding chirp mass, the nature of GW170817 is inconclusive in the absence of observing final coalescence at high GW frequencies (Coughlin & Dietrich 2019). For NS–NS coalescence, numerical simulations (e.g., Baiotti & Rezzolla 2017) show that gravitational radiation effectively satisfies the canonical model signal of binary coalescence in a run-up to about 1 kHz, beyond which the amplitude levels off and ultimately decays as the two stars merge into a single object at a maximal frequency ~ 3 kHz. In contrast, NS–BH mergers include tidal break-up (Lattimer & Schramm 1976). In a brief epoch of hyper-accretion, the BH would be near-extremal with a remnant of NS debris to form a torus outside its innermost stable circular orbit (ISCO). This process is marked by gravitational radiation switching off early on at a frequency 500–1500 Hz (Vallisneri 2000; Etienne et al. 2009; Faber 2009; Ferrari et al. 2010) and possibly quasi-normal mode oscillations at yet higher frequencies (e.g., Yang et al. 2018).

Here, we report on the energy output \mathcal{E} in gravitational radiation post-merger that appears as a descending chirp of

extended emission (EE) marking spin-down of a compact remnant to binary coalescence at a Gaussian equivalent level of confidence of 4.2σ (van Putten & Della Valle 2019). We give a robust estimate of \mathcal{E} using response curves determined by signal injection experiments in data of the LIGO detectors at Hanford (H1) and Livingston (L1). \mathcal{E} introduces a new calorimetric constraint that may break the degeneracy of an NS or BH central engine.

\mathcal{E} reported here points to the core collapse of the merged NS produced in GW170817, inheriting its angular momentum J while greatly increasing the associated spin-energy E_j through collapse into a Kerr BH (Kerr 1963).

After our injection experiments were initiated, we learned of an independent analysis of energy considerations by single-template injections, pointing qualitatively to similar energies without, however, identifying the origin of our EE (Oliver et al. 2019).

2. \mathcal{E} from Pipeline Response Curves

We set out to determine response curves of our search pipeline by signal injections into LIGO data (Vallisneri et al. 2015; Figures 1–2), including whitening, butterfly filtering, and image analysis of merged (H1,L1) spectrograms (Appendix). Whitening occurs by normalizing the Fourier spectrum over an intermediate bandwidth of 2 Hz, showing GW170817 more clearly than without whitening (van Putten & Della Valle 2019).

We recall that GW170817 is observed as an *ascending chirp* signifying the merger of two compact stars with a time of coalescence $t_c = 1842.43$ s followed by GRB 170817A across a gap of 1.7 s. In our injection experiments with LIGO data, we include a model DNS with the same chirp mass $\mathcal{M}_c = 1.188M_\odot$ as GW170817 (Figure 2) at time of coalescence of about 1818 s, producing two side-by-side ascending chirps (Figure 3). A double NS system (DNS) is described by binary masses M_1 , M_2 , $\mu = M_1M_2/M$, $M = M_1 + M_2$, at orbital separation a and orbital frequency

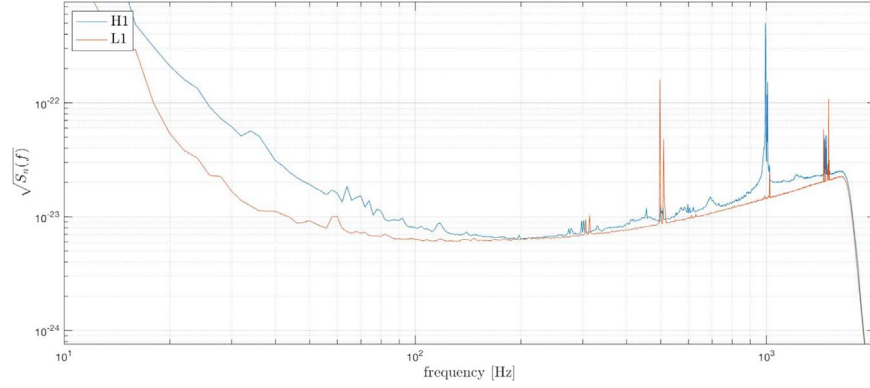


Figure 1. H1 and L1 detector noise shown by the square root of spectral energy density $S_n(f)$ (at the reduced sampling rate 4096 Hz, with a glitch in L1 removed by LIGO) for an epoch of 2048 s containing GW170817 (top panel). Spikes are violin modes associated with the suspension of optics. Frequencies up to about 1700 Hz can be used in injection experiments. H1 and L1 detector noise is very similar during GW170817.

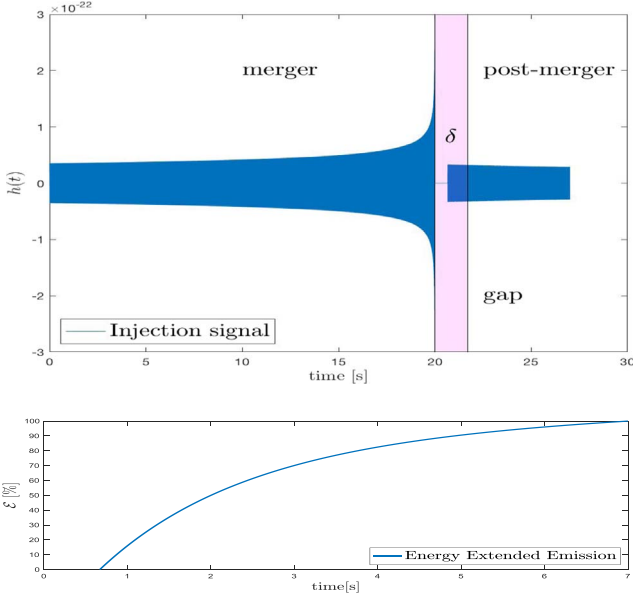


Figure 2. Injection signal comprising a double NS system (DNS) merger and a post-merger branch separated by a delay $\delta = 0.67$ s inside the gap of 1.7 s between GW170817 and GRB 170817A. The post-merger signal has a duration of 7 s at with relatively flat strain $h \propto f^\alpha$ ($\alpha = 0.1$).

$\Omega \simeq c\sqrt{R_g/a^3}$ ($a \gg R_g$), where $R_g = GM/c^2$ is the gravitational radius of the system, given the velocity of light c and Newton's constant G . This merger chirp has a quadrupole GW frequency $f_{\text{GW}} = \pi^{-1}\Omega$

$$f_{\text{GW}}(t) = A(t_c - t)^{-\frac{3}{8}} \quad (t < t_c), \quad (1)$$

$[A] = \text{s}^{-5/8} \text{ Hz}$, with strain $h(t) = (4\mu/D)(M\Omega)^{\frac{2}{3}}$, $h(t) \simeq 1.7 \times 10^{-22}(M/3M_\odot)(D/40 \text{ Mpc})^{-1}(f_{\text{GW}}/250 \text{ Hz})^{\frac{2}{3}}$ and $L_{\text{GW}} = (32/5)(\mathcal{M}_c\Omega)^{10/3}L_0$, where $L_0 = c^5/G \simeq 200,000M_\odot c^2 \text{ s}^{-1}$ (e.g., Ferrari et al. 2010). For GW170817, $A \simeq 138 \text{ s}^{-5/8} \text{ Hz}$. Up to 260 Hz in both H1 and L1, L_{GW} reaches $1.35 \times 10^{50} \text{ erg s}^{-1} \simeq 7.5 \times 10^{-5}M_\odot c^2 \text{ s}^{-1}$, i.e., $4 \times 10^{-10}L_0$. While small compared to $10^{-5}L_0$ of GW150914 at similar frequency, GW170817 produced the largest strain observed by its proximity of $D \simeq 40 \text{ Mpc}$. It emitted $E_0 = 0.43\%M_\odot c^2$ over 200–300 Hz with $h = (1.4\text{--}1.8) \times 10^{-22}$ over $\Delta t \simeq 0.25 \text{ s}$ across $74 \text{ km} < r < 97 \text{ km}$ assuming $M_1 = M_2$.

A merged (H1,L1) spectrogram shows EE post-merger below 700 Hz in the form of an exponential feature

$$f_{\text{GW}}(t) = (f_s - f_0)e^{-(t-t_s)/\tau_s} + f_0 \quad (t > t_s) \quad (2)$$

with the observed $\tau_s = 3.01 \pm 0.2 \text{ s}$, $t_s = 1843.1 \text{ s}$, $f_s = 650 \text{ Hz}$, and $f_0 = 98 \text{ Hz}$. For illustrative purposes, we note that the isotropic equivalent strain $h = L_{\text{GW}}^{1/2}/(\Omega D)$ ($c = G = 1$ in geometrical units) for the chirp mass of a small quadrupole mass moment $\zeta = \delta m/M$ gives $h(t) \simeq 2.7 \times 10^{-23}(\zeta/3\%)(D/40 \text{ Mpc})^{-1}(f_{\text{GW}}/650 \text{ Hz})^{2/3}$, $L_{\text{GW}} \simeq 2 \times 10^{52}(\zeta/3\%)^2(10M/r)^5 \text{ erg s}^{-1} \simeq 1\%M_\odot c^2/\text{s}^{-1}$.

Next we use phase coherent injections with frequency evolution (2) (see Appendix). No change in the results listed below are found after including phase incoherence by a Poisson distribution of random phase jumps over intermediate time-scales, down to the duration $\tau = 0.5 \text{ s}$ of our butterfly templates. $\tau = 0.5$ appears intrinsic, as the EE feature tends to fade out as τ approaches 1 s.

The total energy output $\mathcal{E} = \int_0^T L_{\text{GW}} dt$ is computed numerically as sums $\mathcal{E} = E_0 K^{-1} \sum \nu_i^2 h_i^2$ (samples at t_i , $i = 1, 2, \dots, n$) covering a post-merger interval of duration T , where $K = \sum \nu_{0,j}^2 h_{0,j}^2$ (samples at t_j , $j = 1, 2, \dots, m$) is a reference sum with energy E_0 over a duration T_0 , and $\nu_i = f_{\text{GW}}(t_i)$ denotes GW frequency. E_0 is conform quadrupole emission in the same orientation as the progenitor binary by the conservation of orbital-to-spin angular momentum in transition to its remnant. Blind to any model in particular, we consider injections with power-law strain $h \propto f^\alpha$ with $T = 7 \text{ s}$.

Figure 3 shows the outcome of a signal injection alongside GW170817EE after a calibration $C_h = 0.7$ for observed-to-true strain due to non-ideal H1 and L1 detector orientations relative to GW170817. Extended to multiple injections, the results show that there is no interference with the merger signal or with one another.

Figure 4 shows our estimated response curves $\chi(\mathcal{E})$ for $h \propto f^\alpha$ ($0.1 \leq \alpha \leq 1.0$). By $\hat{\chi} \simeq 7.2$ of the EE to GW170817, we infer

$$\mathcal{E} \simeq (3.5 \pm 1)\%M_\odot c^2. \quad (3)$$

For the descending chirp at hand (2), \mathcal{E} mostly derives early on at high f_{GW} with $L_{\text{GW}} \lesssim 1\%M_\odot c^2 \text{ s}^{-1}$ (Figure 2).

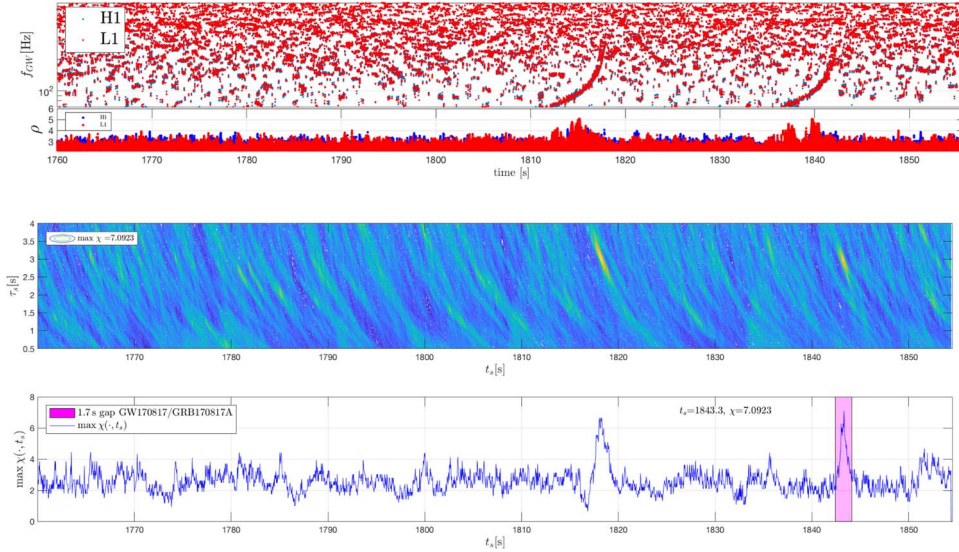


Figure 3. Upper panel: (H1,L1) spectrogram merged by frequency coincidences of butterfly filtering showing GW170817 ($t_c = 1842.43$ s) alongside a model signal ($t_c \simeq 1818$ s). GW170817 appears with $\mathcal{E} \simeq 3\%M_\odot c^2$ in EE. Included is $\rho = \sqrt{\text{SNR}}$ in the tail >2 of butterfly output of H1 and L1. Middle and lower panels: χ -image analysis of EE in the (H1,L1) spectrogram over parameters (t_s, τ_a) for initial and final frequencies (f_s, f_0) = (650, 98) Hz with a similar EE signal strength of the signal injection to that of GW170817 ($t_s = 0.67(\pm 0.03)$ s) measured by the peak value of the indicator χ .

3. Enhanced E_J in Collapse to a BH

\mathcal{E} in (3) is a significant amount of energy, exceeding the merger output observed up to about 300 Hz, emitted as a descending chirp over a secular timescale of seconds with $f_{\text{GW}} < 700$ Hz far below the characteristic frequency $c/R_S \simeq 30$ kHz of the Schwarzschild radius $R_S = 2R_g$. Important energies also appear in GRB 170817A and mass ejecta (e.g., Mooley et al. 2018a, 2018b). Of these, \mathcal{E} and f_{GW} will serve as primary observational constraints on the remnant, i.e., E_J of a rapidly spinning merged NS or rotating BH.

While a long-lived NS might be luminous in gravitational radiation through a baryon-loaded magnetosphere (Appendix), its spin frequency $f_s = (1/2)f_{\text{GW}}$ inferred from our EE is less than one-fifth the break-up spin frequency of about 2 kHz. This modest initial spin limits E_J to below $0.5\%M_\odot c^2$, and probably somewhat less based on more stringent limits (e.g., Haensel et al. 2009; Oliver et al. 2019).

However, E_J greatly increases due to the core collapse of the merged NS in the immediate aftermath of GW170817, here at time of core collapse about or prior to $t_s = 0.67(\pm 0.03)$ s post-merger (Figure 3), where the 30 ms refers to our time-step in t_s . By the Kerr (1963) metric,

$$E_J = 2Mc^2 \sin^2(\lambda/4) \lesssim 1M_\odot c^2 (M/3M_\odot) \quad (4)$$

in terms of $a/M = \sin \lambda$, $J = a \sin \lambda$. This potentially enormous energy reservoir amply accounts for \mathcal{E} even at modest efficiency η , provided that a mechanism is in place to tap and convert E_J into gravitational radiation. Moderate frequencies $f_{\text{GW}} < 700$ Hz can be realized in catalytic conversion into quadrupole emission by a non-axisymmetric disk or torus that is sufficiently wide or geometrically thick. Exhausting E_J , a descending chirp results from the expansion of the ISCO during BH spin-down.

4. \mathcal{E} Estimate from BH Spin-down

To add some concreteness, we estimate η in the spin-down of an initially rapidly rotating BH, losing J to matter in Alfvén

waves through an inner torus magnetosphere (van Putten 1999, 2001). By heating, a non-axisymmetric thick torus is expected to generate frequencies correlated to but below those of a thin torus about the ISCO (Coward et al. 2002). In geometrical units, an extended torus produces emission from an orbital radius $r \equiv zR_g$ at twice the local orbital frequency, i.e., $f_{\text{GW}} \simeq c\pi^{-1}\sqrt{R_g/r^3}$. Asymptotic scaling relations for large radii (modest η ; van Putten & Levinson 2003) show $L_{\text{GW}} \sim 10^{52}$ erg s $^{-1}$ for a non-axisymmetric torus with mass ratio $\sigma = M_T/M \simeq 0.1$. Accompanying minor output can be found in MeV neutrinos and $E_w \simeq \eta^2 E_J$ in magnetic winds (van Putten & Levinson 2002a, 2002b, 2003)—most of E_J is dissipated unseen in the event horizon, increasing in area via the Bekenstein–Hawking entropy (van Putten 2015). The observed 150 Hz $< f_{\text{GW}} < 700$ Hz indicates an effective radius of a quadrupole mass moment that is initially about three times the ISCO radius (Figure 5), suggesting a relatively thick torus. f_{GW} decreases with z because of the expansion of the ISCO during BH spin-down.

Via the numerical integration of this spin-down process, the catalytic conversion of E_J gives (Figure 5)

$$\mathcal{E} \simeq \langle \eta \rangle E_J \simeq 3.6 - 4.3\%M_\odot c^2 \quad (5)$$

for canonical values of initial a/M , depending somewhat on the start frequency $f_s = 600\text{--}700$ Hz, which is consistent with (3) inferred from $\chi(\mathcal{E})$.

The model estimate (5) uses effective values of disk mass m and K throughout. This does not readily predict $h(f_{\text{GW}})$ or the observed exponential feature (2), as m and K will be time dependent and vary with z . Effective mean values is used only for our present focus on total energy output.

While the nature of GW170817 in the chirp up to 300 Hz is somewhat inconclusive (Coughlin & Dietrich 2019), \mathcal{E} provides a novel calorimetric constraint on its remnant. \mathcal{E} in (3) challenges a hyper-massive NS (Oliver et al. 2019) yet is naturally accommodated by (5) in core collapse to a Kerr BH.

In converting E_J , \mathcal{E} is accompanied by MeV neutrinos and magnetic winds (van Putten & Levinson 2003), which is

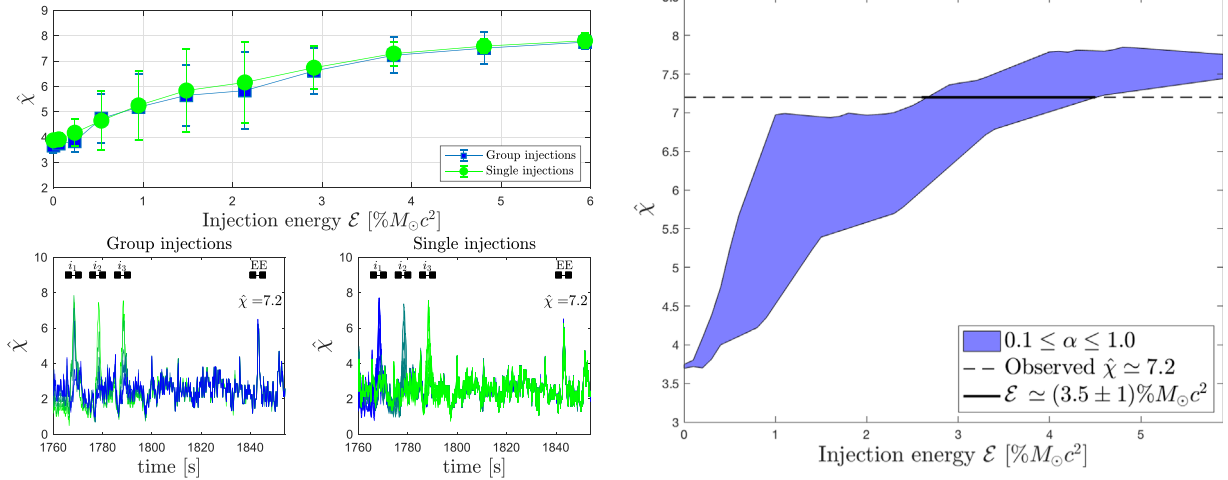


Figure 4. Left panel: response peaks $\hat{\chi}(\mathcal{E})$ of signal injections $h \propto f^\alpha$ ($\alpha = 0.1$) in a merged (H1,L1) spectrogram covering GW170817 by the indicator function $\hat{\chi}$ in χ -image analysis as a function of energy input \mathcal{E} . The response curve (green, blue curves; top panel) determined by injections at instances (i_1, i_2, i_3) about 1 minute before GW170817 (lower panels) is the same by grouped (left bottom) or single (right bottom) injections, demonstrating non-interference between different signals. Color (blue to green) indicates injection strength in group injections and injection position in single injections. Scatter in $\hat{\chi}(E)$ by noise fluctuations appears least at i_1 . Right panel: EE to GW170817 is observed at $\hat{\chi} \simeq 7.2$ (dashed blue line) intersected by $\hat{\chi}(\mathcal{E})$ from i_1 to power-law injections $h \propto f^\alpha$ ($\alpha = 0.1, 0.2, \dots, 1.0$) (solid blue line).

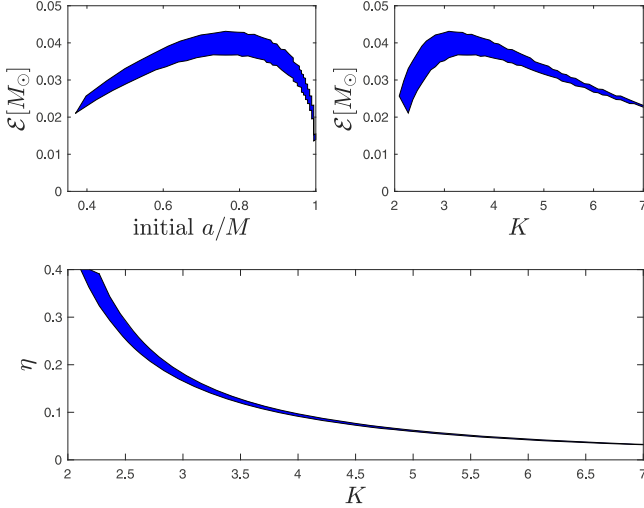


Figure 5. Model prediction of \mathcal{E} in a descending chirp from a non-axisymmetric torus of effective radius K times the ISCO radius around a BH of initial mass $M_0 = 3M_\odot$, converting E_J into gravitational radiation at moderate efficiencies η . The boundaries of the thick curve refers to GW frequencies $f_s = 600\text{--}700$ Hz at start time t_s .

consistent with evidence for BH spin-down in normalized light curves of long GRBs (van Putten 2012).

5. Multi-messenger EE

Starting with the merged NS from a DNS, a time of collapse about or prior to $t_s \simeq 0.67(\pm 0.03)$ s (Figure 3) appears consistent—perhaps in mild tension—with the recently estimated time of collapse $0.98^{+0.31}_{-0.26}$ s based on jet propagation times and the mass of blue ejecta (Gill et al. 2019).

Sustained by Alfvén waves outward over an inner torus magnetosphere, a torus developing a dynamo with magnetic field $B = O(10^{16})$ G limited by dynamical stability over the lifetime of BH spin (van Putten & Levinson 2003) gives a characteristic timescale for the lifetime of rapid spin of the BH,

and hence of the BH-torus system

$$T_s \simeq 1.5 \text{ s} \left(\frac{\sigma}{0.1} \right)^{-1} \left(\frac{z}{6} \right)^4 \left(\frac{M}{3M_\odot} \right), \quad (6)$$

which is consistent with the duration T_{90} (90% of gamma-ray counts over background) of GRB 170817A. Over this secular timescale, the BH gently relaxes toward a nearly Schwarzschild BH as the ISCO expands. The relatively baryon-poor environment of the BH is ideally suited for it to also launch an ultra-relativistic baryon-poor jet within a baryon-rich disk or torus wind with (van Putten & Levinson 2003)

$$E_j \simeq \frac{E_J}{4z^4} \simeq 5 \times 10^{50} \text{ erg}, \quad E_w \simeq \eta^2 E_J \simeq 4 \times 10^{51} \text{ erg}, \quad (7)$$

consistent with $E_j \sim 10^{49\text{--}50}$ erg and $E_k = (1/2)M_{\text{ej}}v^2 \simeq 4.5 \times 10^{51}$ in the relativistic ejecta of GRB 170817A and $M_{\text{ej}} \simeq 5\%M_\odot$ of mass ejecta at mildly relativistic velocities $v \simeq 0.3c$ (Mooley et al. 2018a, 2018b). Emission terminates abruptly as the remnant torus collapses onto the BH when $\Omega_H \simeq \Omega_T$ ($f_{\text{GW}} \simeq 10^2$ Hz).

6. Conclusions

$\mathcal{E} \simeq (3.5 \pm 1)\%M_\odot c^2$ in EE, measured by $\hat{\chi}(\mathcal{E})$ through signal injections (Figure 4), gives a powerful calorimetric constraint on the central engine. This outcome points to a Kerr BH formed in the core collapse of the merged NS in the immediate aftermath of GW170817.

At $f_{\text{GW}} < 700$ Hz, our \mathcal{E} is consistent with post-merger bounds of LIGO (Abbott et al. 2017c, between the dashed lines $E_{\text{gw}} = 0.01\text{--}0.1M_\odot c^2$ in Figure 1) and Oliver et al. (2019). With the E_J of a Kerr BH, the concerns of Oliver et al. (2019) on the detectability of EE are unfounded. Accurate time-integration of the complex scaling $L_{\text{GW}} \propto (f_{\text{GW}} [h/C_h])^2$ highlights the need for measurement by signal injection, for which a one-frequency estimate of h_{H1} alone (van Putten & Della Valle 2019) now appears inadequate.

Core collapse greatly enhances E_j in J inherited from the merged NS up to about $1M_\odot c^2$ in a $\sim 3M_\odot$ BH. It amply accommodates \mathcal{E} even at modest efficiencies in conversion to \mathcal{E} over durations of seconds (Figure 5). Accompanying minor emissions (7) in mass ejecta from the torus and ultra-high-energy emission from the BH agree quantitatively with observational constraints on the associated kilonova and GRB 170817A. GW170817 is too distant, however, to probe any MeV neutrino emission (Bays et al. 2012) in its MeV torus (van Putten & Levinson 2003).

Conceivably, EE does not completely exhaust E_j , permitting low-luminosity latent emission including minor output in baryon-loaded disk winds and low-luminosity jets. While outside the scope of this Letter, this might be an alternative to the same from a long-lived NS remnant that accounts for AT0217gfo (Ai et al. 2018; Li et al. 2018; Yu et al. 2018; Piro et al. 2019).

At improved sensitivity, LIGO-Virgo O3 observations may significantly improve our ability to identify the nature of binary mergers involving an NS—including the tidal break-up in an NS–BH merger—and their remnants that might also be found in core-collapse supernovae and, possibly, the accretion-induced collapse of white dwarfs.

The authors thank the reviewer for a detailed reading and constructive comments. The first author gratefully thanks ACP, Aspen, CO, GWPop 2019 (PHY-1607611), and AEI, Hannover, where our signal injections were initiated in discussions with M. Alessandra Papa and B. Allen. We also thank A.V. Mukhanov and J. Kanner for constructive comments. We acknowledge use of the data set 10.7935/K5B8566F of the LIGO Laboratory and LIGO Scientific Collaboration, funded by the U.S. NSF, and support from NRF Korea (2015R1D1A1A01059793, 2016R1A5A1013277, 2018044640) and MEXT, JSPS Leading-edge Research Infrastructure Program, JSPS Grant-in-Aid for Specially Promoted Research 26000005, MEXT Grant-in-Aid for Scientific Research on Innovative Areas 24103005, JSPS Core-to-Core Program, Advanced Research Networks, and ICRR.

Appendix Supporting Data

Winjection.m, whitening and signal injection (Figure 2), doi:[10.5281/zenodo.2613112](https://doi.org/10.5281/zenodo.2613112).

EEE.m, estimated energy and efficiency of EE (Figure 5), doi:[10.5281/zenodo.2613105](https://doi.org/10.5281/zenodo.2613105).

Our broadband extended GW emission (BEGE) pipeline aims for unmodeled ascending and descending chirps with a choice of an intermediate timescale of phase coherence $0 < \tau \lesssim 1$ s, expected from extreme transient events exhausting E_j of their central engine in seconds.

1. Butterfly filtering is matched filtering against a bank of time-symmetric chirp-like templates of intermediate duration τ , densely covering a domain in $(f(t), |df(t)/dt| \geq \delta)$ for some choice of $\delta > 0$. Single-detector spectrograms are extracted as scatter plots of correlations $\rho(t, f_c)$ between data segments (here, of 32 s duration) and time-symmetric chirp-like templates with central frequency f_c .
2. To reduce noise in deep searches ($\kappa = 2$), spectrograms are merged by frequency coincidences ($|f_{c,H1} - f_{c,H2}| < \Delta f$) to conform causality: Δf is about $|df(t)/dt| \delta t$, where $\delta t = 10$ ms is the (maximal) signal propagation time

between H1 and L1. We obtain satisfactory results with $\Delta f = 10$ Hz (Figure 3).

3. Candidate features (Figure 3) are evaluated by counting “hits:” $\chi(\rho > \kappa\sigma)$ by H1&L1 over strips about a given family of curves—normalized to $\hat{\chi}$. For EE feature to GW170817, we use (2), giving $\hat{\chi}(t_s, f_s, f_0, \tau_s)$. The strip is of finite width ($\Delta f = 10$ Hz, $\Delta t = 0.1$ s), discretized with $\Delta t_s = 0.030$ s and, for background statistics, over $N = 16$ steps in each parameter gathered from 1956 s of clean LIGO data in a scan over a total of 256M parameters ($N^3 = 4096$, $\Delta t_s = 30$ ms; van Putten & Della Valle 2019).

The merged NS produced by GW170817 may briefly emit GWs through a magnetosphere with field B , baryon-loaded with M_b by dynamical mass ejecta and MeV-neutrino winds (e.g., Perego et al. 2014), by a quadrupole moment μ along its magnetic spin-axis misaligned with J (Kalapotharakos et al. 2012), extending out to l of its light cylinder. At Alfvén velocity $c_A = B/\sqrt{4\pi\rho}$, $B = B_{16}10^{16}$ G with matter density ρ , μ greatly exceeds that of B in a vacuum (Hacyan 2017). In geometrical units ($c = G = 1$), the polar flux axis radiates like a rod with (Wald 1984) $L_{\text{GW}} = (32/45)\mu^2\Omega^6 \simeq (32/45)(m\Omega)^2$, with $\mu = ml^2$. A star of mass M , radius R , and Newtonian binding energy $W = M^2/(2R) \simeq 0.15$ generally satisfies $M \gg W \gg E_j \gg E_{\text{turb}} \gg E_B$ for turbulent motions E_{turb} and $E_B = (1/6)B^2R^3$. Hence, $E_B = (E_{\text{rot}}/W)(E_{\text{turb}}/E_{\text{rot}})(E_B/E_{\text{turb}})W \simeq 10^{-4}M$ for fiducial ratios of 0.1 for each factor with corresponding $B \simeq 4 \times 10^{16}$ G. M_b enhances $m \simeq f_B E_B$ by $2\beta_A^{-2}$, $\beta_A = c_A/c$, where $f_B \simeq 0.5$ for a dipole field. Accordingly, $L_{\text{GW}} \simeq (32/45)(m\Omega\beta_A^{-2})^2 \simeq 2 \times 10^{52}(B_{16}/(\beta_A/0.1))^4(f_s/350 \text{ Hz})^2 \text{ erg s}^{-1}$ at rapid spin when l is a few times R . Such a burst would be short by canonical bounds on E_j of an NS.

E_j increases dramatically in the continuing core collapse into a BH. A numerical estimate of \mathcal{E} derived from the catalytic conversion of $E_j = 2M \sin^2(\lambda/2) \lesssim 0.29M$ at $a/M = \sin \lambda$ (non-extremal) at modest efficiency at orbital angular velocity $\Omega_T = \pi f_{\text{GW}}$ relative to $\Omega_H = \tan(\lambda/2)/(2M)$ of the BH. The estimated initial frequency of ~ 744 Hz at time of coalescence t_c inferred from $t_s = 0.67$ s is below the orbital frequency at which the stars approach the ISCO of the system mass, which is about 1100 Hz at $r \simeq 16$ km. At this point, an equal-mass DNS has $a/M = 0.72 < 1$, which is consistent with numerical simulations (e.g., Baiotti & Rezzolla 2017); this allows collapse to a $\sim 3M_\odot$ Kerr BH with $E_j \simeq 24\%M_\odot c^2$. For a torus radius K times the ISCO radius, Figure 5 shows the result of integration of the equations describing spin-down with a $\mathcal{E} \simeq 3.6\text{--}4.3\%M_\odot$ at aforementioned canonical initial values a/M , which is subject to the observed GW frequency $600 \text{ Hz} < f_{\text{GW}} < 700 \text{ Hz}$ at $t_s = 0.67$ s post-merger. This is consistent with (3).

ORCID iDs

Maurice H. P. M. van Putten  <https://orcid.org/0000-0002-9212-411X>

Massimo Della Valle  <https://orcid.org/0000-0003-3142-5020>

References

- Abbott, B. P., Abbott, R., Abbott, T. D., et al. 2017a, *PhRvL*, **119**, 161101
 Abbott, B. P., Abbott, R., Abbott, T. D., et al. 2017b, *ApJL*, **848**, L13
 Abbott, B. P., Abbott, R., Abbott, T. D., et al. 2017c, *ApJL*, **851**, L16
 Ai, S., Gau, He., Dai, Z.-G., et al. 2018, *ApJ*, **860**, 57

- Baiotti, L., & Rezzolla, L. 2017, *RPPh*, **80**, 096901
- Bays, K., Iida, T., Abe, K., et al. 2012, *PhRvD*, **85**, 052007
- Connaughton, V. 2017, GCN, 21506, 1
- Coughlin, M., & Dietrich 2019, arXiv:1901.06052v1
- Coward, D. M., van Putten, M. H. P. M., & Burman, R. R. 2002, *ApJ*, **580**, 1024
- D'Avanzo, E., Benetti, S., Branchesi, M., et al. 2017, *Natur*, **551**, 67
- Etienne, Z. B., Liu, Y. T., Shapiro, S. L., & Baumgarte, T. W. 2009, *PhRvD*, **79**, 044024
- Faber, J. A. 2009, *CQGra*, **26**, 114004
- Ferrari, V., Gualtieri, L., & Pannarale, F. 2010, *PhRvD*, **81**, 064026
- Freedman, W. L. 2017, *NatAs*, **1**, 0121
- Gill, R., Nathanail, A., & Rezzolla, L. 2019, *ApJ*, in press (arXiv:1901.04138v1)
- Goldstein, A., Veres, B., Burns, E., et al. 2017, *ApJL*, **848**, L14
- Guidorzi, C., Margutti, R., Brout, D., et al. 2017, *ApJL*, **851**, L36
- Hacyan, S. 2017, *RMxF*, **63**, 466
- Haensel, P., Zdunik, J. L., Bejger, M., et al. 2009, *A&A*, **502**, 605
- Kalopotharakos, C., Kazanas, D., Harding, A., & Contopoulos, I. 2012, *ApJ*, **749**, 2
- Kasen, D., Metzger, B., Barnes, J., et al. 2017, *Natur*, **551**, 80
- Kasliwal, M. M., Nakar, E., & Singer, L. P. 2017, *Sci*, **358**, 1559
- Kerr, R. P. 1963, *PhRvL*, **11**, 237
- Lattimer, J. M., & Schramm, D. N. 1976, *ApJ*, **210**, 549
- Li, S.-Z., Liu, L.-D., Yu, Y.-W., & Zhang, B. 2018, *ApJL*, **861**, L12
- Metzger, B. D., Thompson, T. A., & Quataert, E. 2018, *ApJ*, **856**, 101
- Mooley, K. P., Deller, A. T., Gottlieb, O., et al. 2018a, *Natur*, **554**, 207
- Mooley, K. P., Deller, A. T., Gottlieb, O., et al. 2018b, *Natur*, **561**, 355
- Oliver, M., Keitel, D., Miller, A., et al. 2019, *MNRAS*, **485**, 843
- Perego, A., Rosswog, S., Cabezón, R. M., et al. 2014, *MNRAS*, **443**, 3134
- Pian, E., D'Avanzo, P., Benetti, S., et al. 2017, *Natur*, **551**, 67
- Piro, L., Troja, E., Zhang, B., et al. 2019, *MNRAS*, **483**, 1912
- Pozanenko, A. S., Barkov, M. V., Minaev, P. Y., et al. 2018, *ApJL*, **852**, L30
- Savchenko, V., Ferrigno, C., Kuulkers, E., et al. 2017, *ApJL*, **848**, L15
- Smartt, S. J., Chen, T.-W., Jerkstrand, A., et al. 2017, *Natur*, **551**, 75
- Vallisneri, M. 2000, *PhRvL*, **84**, 3519
- Vallisneri, M., Kanner, J., Williams, R., et al. 2015, *JPhCS*, **610**, 012021
- van Putten 2015, *ApJ*, **810**, 7
- van Putten, M. H. P. M. 1999, *Sci*, **284**, 115
- van Putten, M. H. P. M. 2001, *PhRvL*, **87**, 091101
- van Putten, M. H. P. M. 2012, *PThPh*, **127**, 331
- van Putten, M. H. P. M., & Della Valle, M. 2019, *MNRAS*, **482**, L46
- van Putten, M. H. P. M., Guidorzi, C., & Frontera, F. 2014, *ApJ*, **786**, 146
- van Putten, M. H. P. M., & Levinson, A. 2002a, *Sci*, **295**, 1874
- van Putten, M. H. P. M., & Levinson, A. 2002b, *CQGra*, **19**, 1309
- van Putten, M. H. P. M., & Levinson, A. 2003, *ApJ*, **584**, 937
- Wald, R. M. 1984, *General Relativity* (Chicago, IL: Univ. Chicago Press)
- Yang, H., East, W. E., & Lehner, L. 2018, *ApJ*, **856**, 110
- Yu, Y.-W., Liu, L.-D., & Dai, Z.-G. 2018, *ApJ*, **861**, 114